J Mater Sci (2007) 42:5085–5093
DOI 10.1007/s10853-006-0955-1

An experimental investigation of rate-dependent deformation and failure of three titanium alloys

Helen Sarsfield · Li Wang · Nikica Petrinic

Received: 6 March 2006 / Accepted: 6 September 2006 / Published online: 21 March 2007

Abstract The response of three titanium alloys, Ti 6,4, Ti 550 and Ti 6,2,4,6, commonly used in aerospace applications, has been investigated at rates of strain between 10^{-4} and 10^{3} s^{-1} in uniaxial tensile and compressive loading in ambient environment. This work identifies and discusses features of their behaviour that must be captured within material models developed for use in predictive modelling of response to in-service loading. That is, an increase in yield strength with increasing strain rate, a difference in yield strength between tensile and compressive loading regimes and, most importantly, the evolution of damage resulting in failure due to growth of voids in both tension and compression.

Introduction

Titanium and its alloys have long been employed in applications which take advantage of its high specific strength; they are increasingly used in applications where they may be subjected to high rates of loading, such as when sustaining foreign object damage on fan blades in gas turbine engines. The design of aerospace structures relies upon a holistic approach including simulation of manufacturing processes and predictive modelling of response to in-service loading. However, accurate prediction of inelastic deformation and failure of components and structures subjected to complex dynamic loading conditions depends upon the performance of constitutive relationships and equations of state, which relate the material response, in terms of stress, to the applied strain, strain rate and temperature. The accuracy of such predictions is directly related to the quality of experimental data used during the development of the governing equations.

The mechanical behaviour of metals at high strain rates has been investigated for many years, but the majority of effort has been focused on fcc and bcc systems with tests conducted mainly in uniaxial tension. The literature includes work on titanium alloys: Rosen et al. [1] report that the tensile yield stress of titanium alloys increases with increasing strain rate, but only considered strain rates up to 100 s^{-1}. Zhou and Chew [2] considered uniaxial tensile tests of titanium over a range of quasi-static loading rates, from $10^{-5}s^{-1}$ to $10^{-1}s^{-1}$, and report that the strength of Ti 6,4 increases with increasing strain rate but at the expense of ductility. El-Magd et al. [3] used the results of compression tests to investigate the constitutive modelling of three different alloys including one titanium alloy, and the strain rate and temperature dependence of the flow stress. They found that the flow stress in dynamic tests is higher than in quasi-static tests and that the difference increases with increasing temperature; when combined with earlier work by MacDougall [4], this highlights the significance of the temperature function in material models over a range of strain rates.

This paper describes the results of an experimental investigation into the behaviour of three titanium alloys, Ti 6,4, Ti 550 and Ti 6,2,4,6 subjected to both tensile and compressive loading at ambient temperature. It focuses on the aim of using the results of mechanical testing and subsequent microscopic examination to characterise the deformation behaviour of the alloys such that numerical

H. Sarsfield (✉) · L. Wang · N. Petrinic
Department of Engineering Science, University of Oxford, Parks Road, Oxford OX1 3PJ, UK
e-mail: helen.sarsfield@eng.ox.ac.uk

models may be developed which capture the observed aspects of the materials' behaviour. The results of the experimental investigation presented here are part of a much wider body of work aimed at enabling development and validation of numerical methods for predictive modelling of deformation and failure in materials subjected to impact loading. This paper presents a summary of findings for three widely used alloys, thus providing the basis for comparison against results obtained using both alternative experimental techniques and numerical methods.

Experimental approach

Materials

Commercially pure titanium undergoes an allotropic transformation from hcp (α-Ti) to bcc (β-Ti) at about 882 °C. The details of the composition of the $\alpha + \beta$ alloy, used in each family of tests are given in Table 1. Ti 6,4 is a versatile medium strength alloy, which exhibits good tensile properties at room temperature, creep resistance up to 325 °C and excellent fatigue strength. Ti 550 has superior room and elevated temperature tensile strength and fatigue strength compared to Ti 6,4 it is creep resistant up to 400 °C. Ti 6,2,4,6 was developed by Pratt and Whitney, and is known for its creep and oxidation resistance, it is the preferred high temperature alloy for gas turbine engine applications in the United States [5].

The Ti 550 and Ti 6,2,4,6 specimens were machined from 9.0 mm thick forged sections whereas the Ti 6,4 specimens were cut from 20.0 mm cross-rolled sheet. Further details on the processing route are commercially sensitive and, as such, have not been divulged to the researchers.

Mechanical testing

This investigation incorporates three families of tests, at three different rates of strain, in both tension and compression. The tests were conducted using:

(a) screw driven loading machine at strain rates of 10^{-4} s^{-1},
(b) hydraulic rig capable of achieving strain rates of 10^{2} s^{-1},
(c) standard tensile and compressive Split-Hopkinson systems for strain rates of up to 10^{4} s^{-1}.

Table 1 The chemical composition (wt%) of the titanium alloys

Material	Ti	Al	V	Sn	Zr	Mo	Si
Ti 6,4	90	6	4				
Ti 550	85.9–92.2	3–5		1.5–2.5		3–5	0.3–0.7
Ti 6,2,4,6	82	6		2	4	6	

Tensile specimens were cylindrical rods with a 3.0 mm diameter, an 8.0 mm gauge length and a 1.5 mm blend radius. The compression specimens were solid cylinders 3.0 mm in diameter and 3.5 mm in length.

At quasi-static and medium rates the testing data collected were limited to force-extension measurements. At higher rates strain gauges on the Split-Hopkinson bars and the assumption of elementary one-dimensional elastic wave propagation theory [6, 7] allow calculation of the resisting force and rate of specimen extension. No remote sensing techniques, such as photogrametry, were employed in this experimental work which means that there can be no quantitative analysis of post instability deformation. Nevertheless, measurement of the final cross-sectional area of the fractured tensile specimens allows estimation of the strain at failure assuming that volume is conserved. Failed compression specimens are not measurable in the same way.

Microstructural characterisation

Optical microscopes allow observation of the fracture surfaces; a scanning electron microscope (SEM) is necessary to allow investigation of the micro-mechanical processes of deformation and fracture, this requires extensive specimen preparation. Specimens were mounted in Woods metal or resin and then sectioned along the loading axis before being polished according to standard metallographic techniques [8]. The final chemical–mechanical polish was with a mixture of colloidal silica and hydrogen peroxide. The reaction product of the hydrogen peroxide with titanium is continuously removed from the sample surface with the silica suspension and leaves the surface free of mechanical deformation.

Results and discussion

Nominal stress–strain curves for the alloys at high (HR), medium (MR) and quasi-static (QS) rates of strain are shown in Fig. 1 (a), (b) and (c). The stress and strain are calculated in the usual way using specimen dimensions, the presented curves are an average of the results obtained from at least three specimens for each test configuration. The graphs plot the results of tests in tension and compression on the same chart. Figure 2 and Table 2(a, b) contain a summary of results and show that the flow stress of the titanium alloys increase with increasing strain rate. The tensile ductility, as measured by elongation, for Ti 6,2,4,6 and Ti 550 is shown to increase with increasing strain rate, in contrast to Ti 6,4 also reported by Zhou and Chew [2]. Observing the fracture surfaces of the Ti 6,4

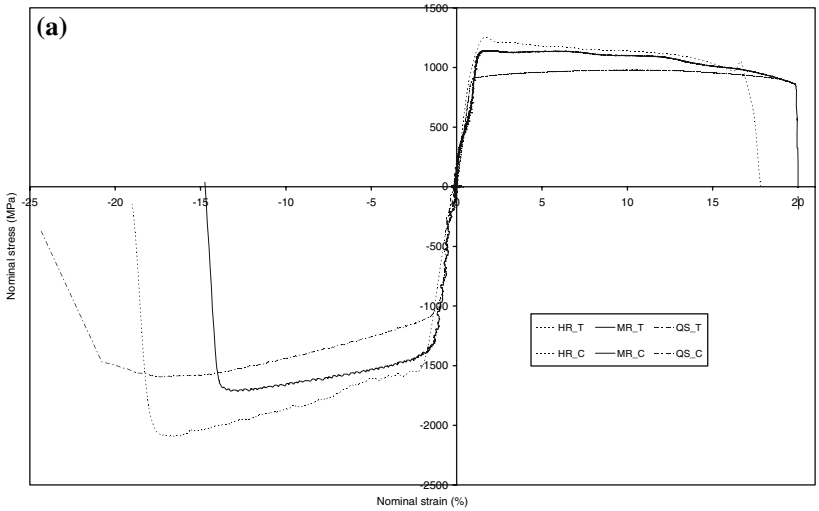

Ti 6,4 nominal stress vs strain

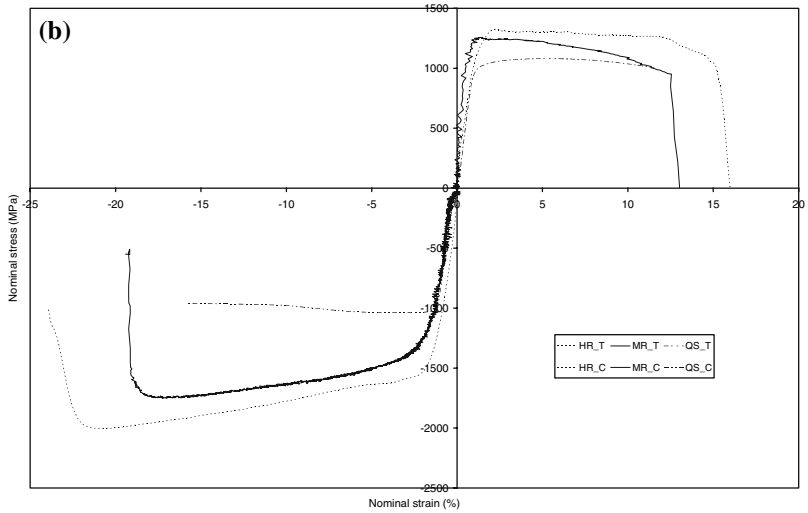

Ti550 nominal stress vs strain

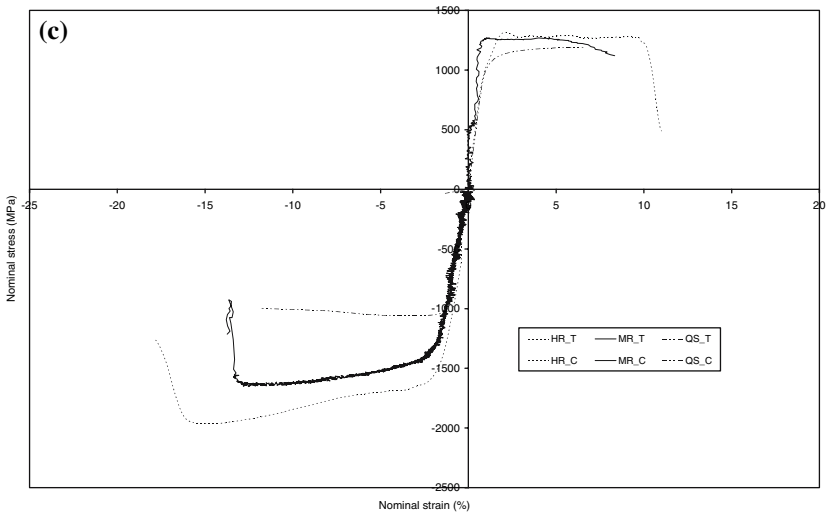

Ti6246 nominal stress vs strain

Fig. 1 **(a)** Ti 6,4 nominal stress versus strain, **(b)** Ti550 nominal stress versus strain, **(c)** Ti6246 nominal stress versus strain

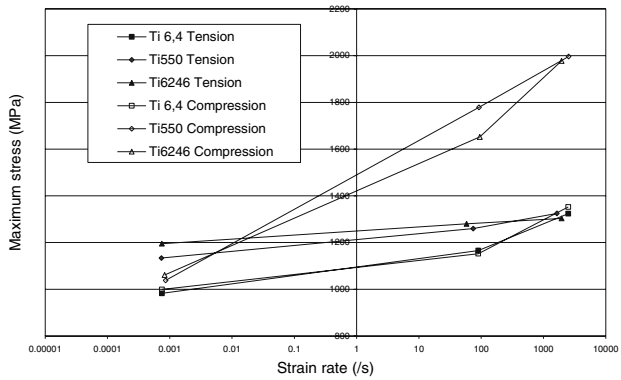

Fig. 2 The strain rate dependent maximum stress

specimens at three different rates, all exhibit dimpled ductile fracture, indicating that there is no significant change in fracture mechanism with deformation rate. The density of the dimples is observed to increase with increasing strain rate, reflecting an improvement in tensile strength and fracture strain. In compression, some of the tests were halted just prior to failure with a view to investigating the evolution of damage.

True stress–true strain curves, calculated from the force-extension data using the commonly applied assumption of incompressibility of plastic deformation, are presented in Fig. 3 (a–c). Interrupted tests indicate that this is valid [9], the damage evolution, due to void growth, is not significant at low levels of plastic strain. However, there can be no quantitative analysis post-instability of deformation because there is no data on the evolution of the specimen dimensions in the neck. An average curve is plotted up to the onset of instability; dimensions of the tensile fracture surfaces are used to plot the failure points.

Figure 4 is a photograph of broken specimens of the three titanium alloys having been tested to failure quasi-statically in tension. The same materials tested at higher rates failed in a similar manner. The fracture surfaces of the Ti 6,4 specimens are dominated by large nearly planar shear lips with a small region of ductile dimples in the centre. The planar ''V'' shape of the failure surfaces is the result of strain localization, which appears to encourage void nucleation and coalescence along planes of maximum deviatoric stress, and this is particularly well illustrated in the scanning electron micrograph of Fig. 5. The region of dimpled ductile fracture is much larger in the Ti550 specimens and occupies most of the fracture surface. The shear lips occur on only a small part of the fracture surface. This is a typical cup and cone ductile fracture surface. In the Ti 6,2,4,6 specimens the fracture surfaces are orientated at approximately 45° to the loading axis—that is, the direction of the maximum shear stress. This difference in fracture behaviour can be attributed to the markedly different phase morphology and manufacturing history.

Table 2a Experimental strain rates achieved and comparison of the mechanical properties in tension

Material	Loading rate (s^{-1})	True strain at failure (%)	True stress at failure (MPa)	UTS (MPa)
Ti 6,4	7.5×10^{-4}	35.5	1,270	983
Ti 6,4	9.0×10^{1}	47.7	1,470	1,170
Ti 6,4	2.5×10^{3}	51.2	1,650	1,460
Ti 550	7.3×10^{-4}	28.9	1,300	1,130
Ti 550	7.5×10^{1}	49.9	1,420	1,260
Ti 550	1.6×10^{3}	45.6	1,610	1,320
Ti 6,2,4,6	7.5×10^{-4}	15.0	1,340	1,200
Ti 6,2,4,6	5.8×10^{1}	26.9	1,380	1,280
Ti 6,2,4,6	1.3×10^{3}	29.7	1,510	1,300

Table 2b Experimental strain rates achieved and comparison of the maximum stress in compression

Material	Loading rate (s^{-1})	Maximum compressive stress (MPa)
Ti 6,4	7.5×10^{-4}	999
Ti 6,4	9.0×10^{1}	1,150
Ti 6,4	2.5×10^{3}	1,260
Ti 550	8.6×10^{-4}	1,040
Ti 550	9.2×10^{1}	1,780
Ti 550	2.5×10^{3}	2,000
Ti 6,2,4,6	8.3×10^{-4}	1,060
Ti 6,2,4,6	9.5×10^{1}	1,650
Ti 6,2,4,6	2.0×10^{3}	1,980

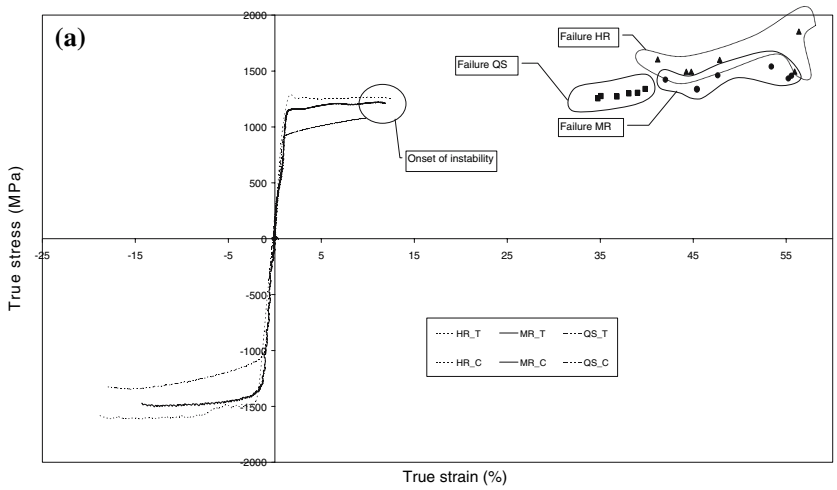

Ti 6,4 True stress vs true strain

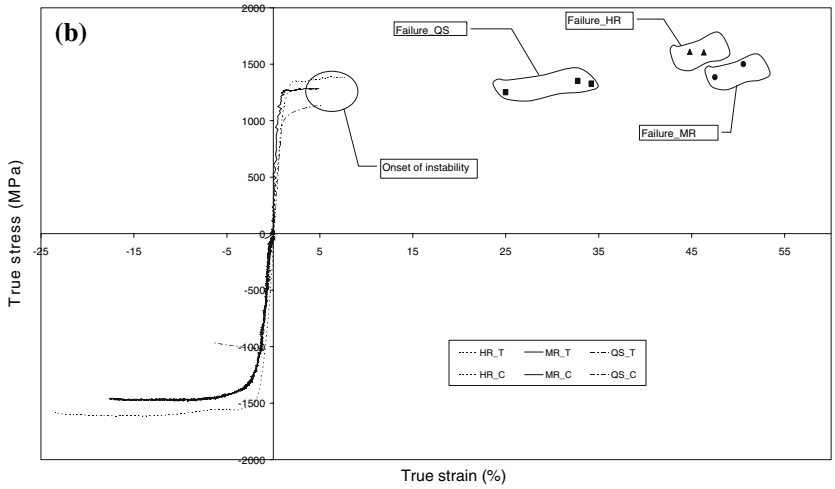

Ti 550 True stress vs true strain

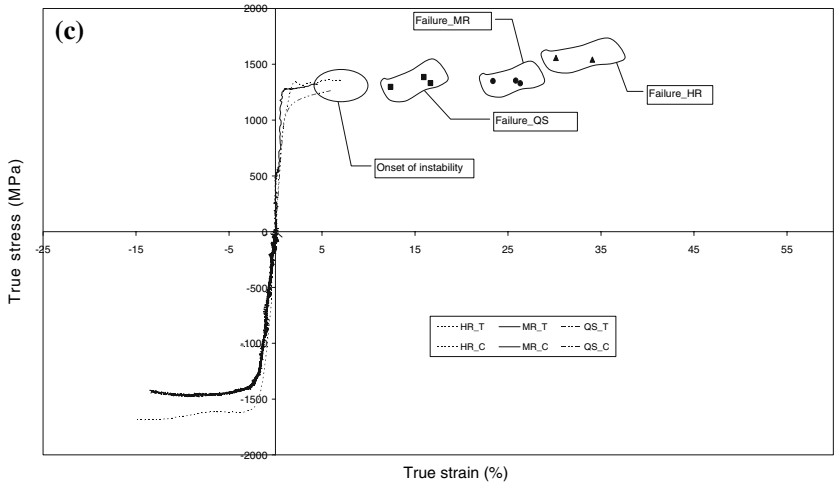

Ti 6,2,4,6 True stress vs true strain

Fig. 3 **(a)** Ti 6,4 true stress versus true strain, **(b)** Ti 550 true stress versus true strain, **(c)** Ti 6,2,4,6 true stress versus true strain

Fig. 4 Failed specimens after the quasi-static strain rate tests

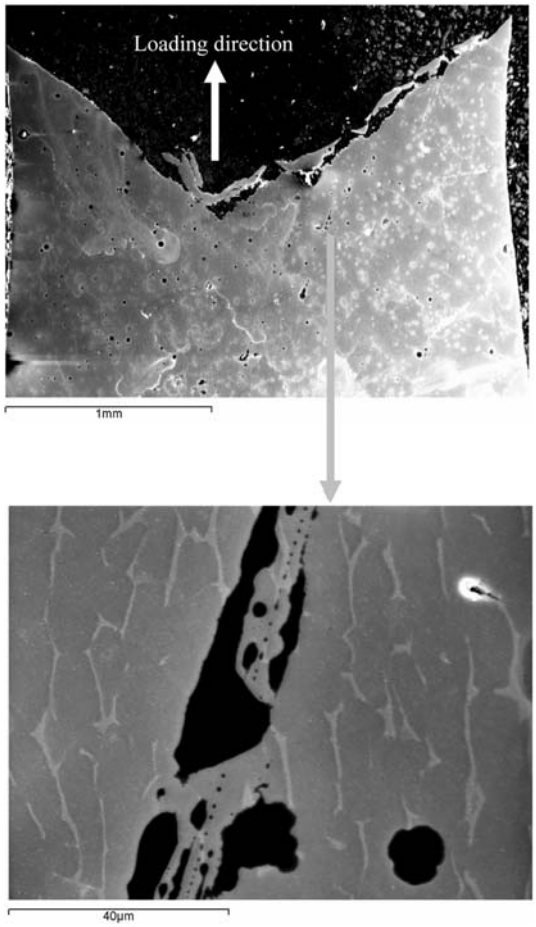

Fig. 5 Void growth and coalescence in a Ti 6,4 specimen having been tested in tension

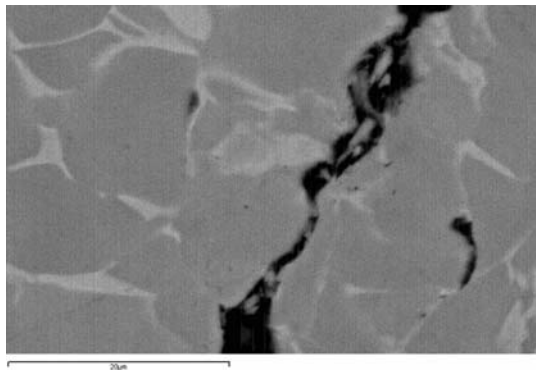

Fig. 6 Microcrack and voids in a Ti 6,4 compression specimen tested at quasi-static rates

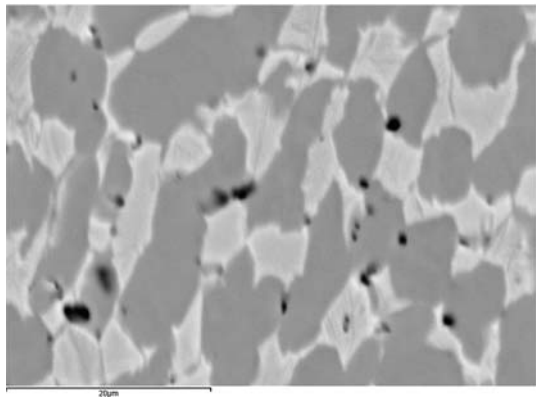

Fig. 7 Microstructure of Ti 550 tensile specimen, close to fracture surface parallel to the base of the image

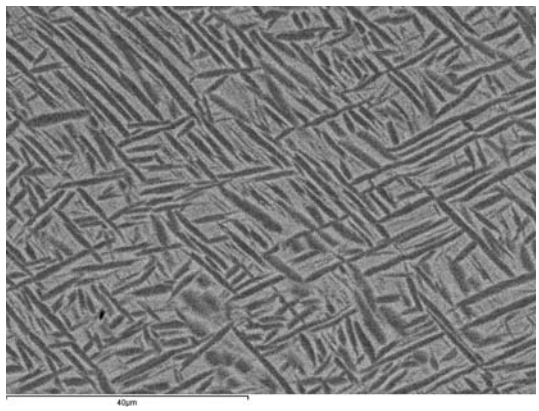

Fig. 8 Microstructure of Ti 6,2,4,6 tensile specimen

Comparing Figs. 6 and 7, it can be observed that Ti 6,4 and Ti 550 have similarly shaped α grains (darker in colour on the secondary electron images), the characteristic grain diameter is of the order of 10 μm to 15 μm. There is a larger volume fraction of β phase in the Ti550, it is only present in thin seams at α grain boundaries in Ti 6,4.

Figure 8 indicates that the Ti 6,2,4,6 has a finer, more needle-like, grain structure than the more equiaxed grains of Ti 6,4 and Ti 550; additionally the grains are much smaller and of the order of 1 μm in width and up to 10 μm in length. Furthermore, the volume fractions of the α and β phases are approximately equal in the Ti 6,2,4,6.

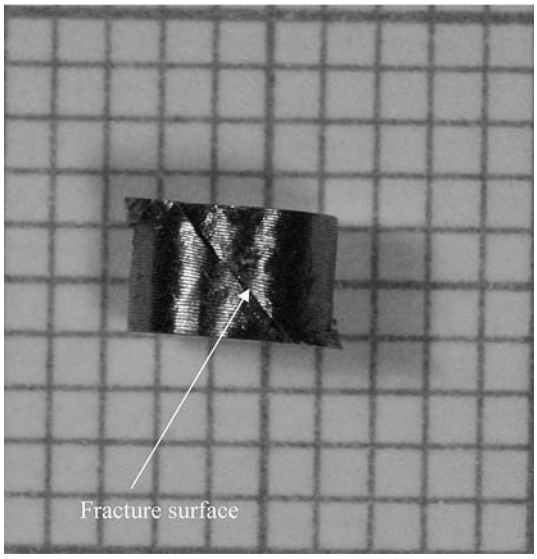

Fig. 9 A failed Ti 6,4 compression specimen having been tested at quasi-static rates

The microscopic examination revealed few connected voids below the fracture surfaces, which illustrates the highly localised and catastrophic character of the final coalescence process. Indeed, any voids found further from the fracture surface appear spherical, they do not elongate as they are not seeing an increase in strain since this is concentrated at the neck, forming the fracture surface. Fewer voids could be observed in the Ti 6,2,4,6 specimen than in the other two alloys, even very close to the fracture surface, comparing Fig. 8 to Figs. 5 and 7.

In compression, localised shear failure is the predominant failure mechanism along a plane at approximately 45° to the loading axis, this is well illustrated for Ti 6,4 in Fig. 9. Remarkably, voids have also been identified in the specimens loaded in compression, Fig. 6. Currently, few material models include the capability to capture void formation in compression. For example, in the Bammann damage model [10] evolution of the damage parameter is only motivated from the growth of spherical voids due to a

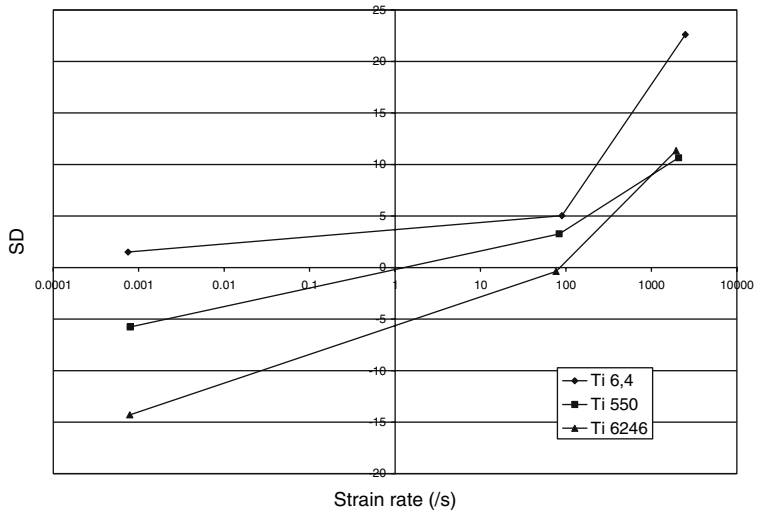

Fig. 10 The strain rate dependent stress differential effect

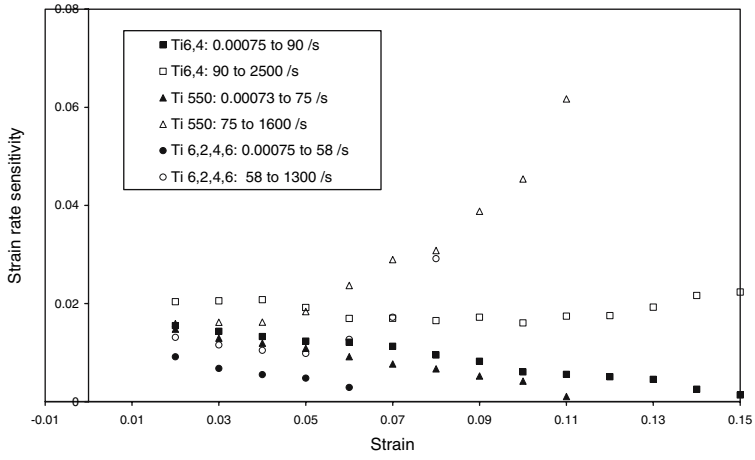

Fig. 11 Variation of strain rate sensitivity with plastic strain for three titanium alloys over two strain rate regions

tensile pressure. Xue et al. [11] completed an investigation of the evolution of multiple adiabatic shear bands in the radial collapse of a thick-walled cylinder under high strain rate deformation; they state that the nucleation of microvoids may be considered as a result of the tensile stress in the radial direction, and that void evolution is comprised of three main stages: nucleation, growth and coalescence. The voids nucleate inside the band and are surrounded by the flow of localised deformation. The sectioning and polishing techniques employed here prevent identification of any shear bands present.

The yield stress and subsequent flow stress of the titanium alloys are higher in compression than tension, Table 2. The stress differential (SD) effect refers to this difference and is well documented [12, 13].

$$\mathrm{SD} = \frac{\sigma_c - \sigma_t}{\frac{1}{2}(\sigma_c + \sigma_t)} \times 100$$

In Zircaloy, which, like titanium, has an hexagonally close packed crystal structure, the effect has been attributed by Snowden [14] to a difference in the ease of twinning in compression and tension due to texture present in the material. Figure 10 plots the SD, expressed as a percentage of the mean of the stress at an offset strain of 2% under compression and tension, against strain rate. The SD effect can be observed in all three alloys, but, significantly, it increases with increasing strain rate, this is in support of Snowden's explanation since the literature [15, 16] describes twin densities increasing with increasing strain rate in titanium alloys. Preliminary work with EBSD techniques has shown that twinning is an important deformation mechanism. Meyers et al. [17] studied shear band formation in α titanium and observed extensive twinning during the high strain rate deformations and concluded that twins may play a role in the initiation of shear bands. The objectives of this study did not include the investigation of shear band formation, but this provides scope for further work.

A general relationship between flow stress and strain rate, at constant strain and temperature, which is useful for further discussion of strain rate dependent behaviour, is [18]:

$$\sigma = C\dot{\varepsilon}^m|_{\varepsilon,T}$$

where m is the strain rate sensitivity, one of the material quantities important to the necking process and C is a constant. Relationships of this form can be found in a number of commonly used material models including:

(a) An empirically based constitutive law in the form proposed by Cowper and Symonds [19].

(b) Physically based constitutive laws proposed by Zerilli and Armstrong which account for strain, strain rate and temperature dependence [20, 21].

The strain rate sensitivity is calculated, at a fixed level of plastic strain and temperature, as:

$$m = \frac{\partial \ln \sigma}{\partial \ln \dot{\varepsilon}} \approx \frac{\Delta \ln \sigma}{\Delta \ln \dot{\varepsilon}} = \frac{\ln \sigma_2 - \ln \sigma_1}{\ln \dot{\varepsilon}_2 - \ln \dot{\varepsilon}_1} = \frac{\ln \frac{\sigma_2}{\sigma_1}}{\ln \frac{\dot{\varepsilon}_2}{\dot{\varepsilon}_1}}$$

Previous work on the strain rate sensitivity of steels [22] and titanium alloys [2] describes how it is seen to decrease with increasing plastic deformation at low strain rates. Figure 11 plots the strain rate sensitivity against tensile strain for two different strain rate regions, quasi-static to medium rate and medium to high rate, for each of the three alloys under investigation. Previously, Zhou and Chew [2] showed that the gradient of a strain rate sensitivity versus strain graph decreases when considering the sensitivity up to strain rates of 0.5 s^{-1}. This experimental work has shown that, at intermediate strain rates, of the order of 100 s^{-1}, the strain rate sensitivity varies much less strongly with increasing plastic strain. Furthermore, as strain rates rise further, the trend is reversed and the strain rate sensitivity can be observed to increase with plastic strain. This is particularly true for Ti 550 and may be attributed to the larger volume fraction of β phase in this alloy than in the others. The β phase has a bcc crystal structure and bcc metals are known to be very strongly rate dependent.

Conclusions

Uniaxial tensile and compressive tests were carried out at three different strain rates, which have enabled comparison of three different widely employed aerospace titanium alloys. All three-exhibit rate dependent behaviour, the flow stress increases with increasing strain rate. Results have been displayed in terms of quantities important for phenomenological numerical modelling of the experiments, that is, true stress versus true strain curves; these illustrate an increase in ductility with increasing strain rate. This represents an improved ability to dissipate energy at high rates of strain such that these alloys are good candidates for use in applications where they may be subjected to high rates of loading. It has been possible to identify a difference in the yield stress in tensile and compressive loading regimes, but, crucially, microscopic examinations have identified void growth in both.

Material models should be developed and validated such that they can capture the observed behaviour. Recommendations from this work would be to explore different mechanisms for the evolution of damage, in both tension

and compression, incorporating the growth of voids and shear bands. The stress–strain curves obtained from this analysis will be necessary for evaluation of yield surfaces. Nominal stress versus nominal strain curves and strain rates provide relevant input for simulations of small-scale experiments, which are required for determination of non-measurable internal variables in material models.

Acknowledgements This work is supported by the UK Engineering and Physical Sciences Research Council and Rolls-Royce plc, who kindly provided the material and inspiration for research. The authors would also like to thank the Department of Materials at the University of Oxford for the use of their microscopy facilities.

References

1. Rosen RS, Paddon SP, Kassner ME (1999) J Mater Eng Perform 8(3):361
2. Zhou W, Chew KG (2002) J Mater Sci 37:5159, Doi: 10.1023/A:1021085026220
3. El-Magd E, Treppmann C, Korthauer M (2003) J Phys IV France 110:141
4. MacDougall DAS, Harding J (1998) Intl J Impact Eng 21(6):473
5. Leyens C, Peters M (eds) (2003) Titanium and titanium alloys: fundamentals and applications. Wiley VCH
6. Petrinic N, Wang L, Elliott BCF (2003) In 7th International Conference on Computational Plasticity, COMPLAS2003, Barcelona
7. Harding J, Wood EO (1960) J Mech Eng Sci 2:88
8. Taylor B, Weidmann E, Metallographic preparation of titanium. In: Struers Application Notes, http://www.struers.com, as on 8 March 2007
9. MacDougall D, Thissel R (2001) Damage accumulation in incipiently failed Ti-6Al-4V under high-rate loading. Materials Science and Technology Division, Los Alamos National Laboratory
10. Bammann DJ et al (1993) In: Jones M, Wierzbicki T (eds) Structural crashworthiness and failure. Elsevier Applied Science
11. Xue Q, Meyers MA, Nesterenko VF (2002) Acta Mater 50:575
12. Mannan SL, Rodriguez P (1973) Scripta Metal 7(10):1069
13. Chait R (1973) Scripta Metal 7(4):351
14. Snowden KU (1971) Scripta Metal 5:467
15. Leclercq SN, Nguy C, Bensussan P (1989) In: International conference of mechanical properties of materials at high rates of strain. Institute of Physics Conference, Oxford
16. Meyers MA, Armstrong RW, Kirchner HOK (eds) (1999) Mechanics and materials: fundamentals and linkages. Wiley Interscience
17. Meyers MA (1994) Dynamic behavior of materials. John Wiley & Sons, Inc., New York
18. Dieter GE (1961) Mechanical metallurgy. McGraw-Hill Book Company
19. Cowper GR, Symonds PS (1958) In Applied mathematics report. Brown University. p 28
20. Zerilli FJ, Armstrong RW (1987) J Appl Phys 61(5):1816
21. Zerilli FJ, Armstrong RW (1992) Acta Metal Mater 40(8):1803
22. Lee W-S, Lam HF (1996) J Mater Process Technol 57:233